Journal of Water Process Engineering 76 (2025) 108110

Contents lists available at ScienceDirect

Journal of Water Process Engineering

journal homepage: www.elsevier.com/locate/jwpe

The hidden challenge of membrane recycling: how drying affects membrane layers?

Bianca Zappulla-Sabio [a], Pierre Le-Clech [b], Ludovic F. Dumée [c,d], Hari Kalathil Balakrishnan [e,f], Hèctor Monclús [a], Gaëtan Blandin [a,*]

[a] LEQUiA, Institute of the Environment, University of Girona, Spain
[b] UNESCO Centre for Membrane Science and Technology, University of New South Wales, Sydney NSW30 2052, Australia
[c] Element Zero, Research and Innovation Department, Malaga, Western Australia, Australia
[d] Nanjing Tech University, Nanjing 210009, China
[e] Khalifa University, Research & Innovation Center for Graphene and 2D Materials (RIC-2D), Abu Dhabi, United Arab Emirates
[f] Khalifa University, Department of Chemical and Petroleum Engineering, Abu Dhabi, United Arab Emirates

ARTICLE INFO

Editor: Sadao Araki

Keywords:
Desalination
Membrane drying
Membrane recycling
Membrane storage
Nanofiltration
Reverse osmosis

ABSTRACT

Improper management or storage after discharge of thin film composite membranes are challenging due to potential drying, which may affect the integrity of the material, decrease the performance and impede their potential recycling for second-hand applications. The impact of drying onto the different layers of thin film composite membranes remain empirical and poorly studied. This work systematically assessed the impact of the drying phenomena on the physical changes across poly(amide) and poly(sulfone) layers by applying drying/rewetting protocols consisting of (1) soaking the membrane in a solvent, (2) drying at 60 °C and (3) rewetting with ethanol. After each step, membrane performance as well as surface characterization were assessed. Severe loss of permeabilities, up to 65 and 90 % for the poly(amide) and the poly(sulfone) layer respectively, were observed. Drying effect was demonstrated to be quickly reversible (1 min soaking in ethanol) for the poly(amide) layer even over several drying-rehydration cycles. Permeability of the poly(sulfone) layer appeared to be permanently impacted due to a possible irreversible surface shrinkage and pores collapsing showing permanent changes in the poly(sulfone) layer. These findings highlight the importance of studying membrane drying to prevent further performance loss, optimize material lifetime, ensure continuity of operation, and enable membrane recycling.

1. Introduction

Thin film composite (TFC) poly(amide) (PA) membranes, developed in the late 1970's [1], represent the current state-of-the-art technology for desalination, primarily due to their ability to operate within varied seawater matrix composition and at high salinity. TFC membranes are characterized by a three-layer structure, including an ultrathin PA layer, generally on top of a porous poly(sulfone) (PSf)-based polymer layer, supported over a non-woven fabric support sheet [2]. The PA layer, produced by interfacial polymerization, is typically dense and highly hydrophilic to control permeability and salt rejection [3]. TFC membranes may be produced for both nanofiltration (NF) and reverse osmosis (RO) applications, by controlling the free volume distribution generated across the active PA layer upon polymerization, allowing for tunable levels of separation form low molecular weight compound to ions [4]. Currently, over 90 % of the membranes used in desalination plants are TFC RO membranes [1,5]. Before operation, TFC membranes modules are usually vacuum-packed, using either wet or dry storage methods to avoid any damage. However, the overall lifetime and recyclability of these membranes can be severely compromised by improper operation or inadequate storage after discharge. In particular, uncontrolled drying after use can directly impact their structural integrity and performance, posing a major challenge for their recycling. To mitigate drying effects and bacterial grown during intermittent operation, membrane suppliers generally provide various recommendations for storage, like soaking the membranes in 1 wt% sodium metabisulfite solution [6]. One other recommendation is to soak the membrane in a 50/50 % ethanol/water or propanol/water solution for 15 min to 2 h

* Corresponding author.
E-mail address: gaetan.blandin@udg.edu (G. Blandin).

https://doi.org/10.1016/j.jwpe.2025.108110
Received 3 March 2025; Received in revised form 7 May 2025; Accepted 5 June 2025
Available online 7 June 2025

when case drying is suspected [6]. However, at an industrial scale, this may not be feasible due to the large amount of ethanol required. Even though drying is a real issue known in industry and membrane manufactures [6], it is poorly studied in the literature and remains empirical without systematic study.

In the literature, the effects of drying on membranes have been primarily investigated in the context of membrane fabrication, where drying plays a crucial role in determining membrane morphology and performance during synthesis [7–10]. However, significantly less attention has been given to the impact of drying on membranes after they have been used in real applications. The consequences of drying on aged or fouled membranes remain poorly understood, highlighting a notable gap in current research and a need for further investigation in this area. Among the few studies reporting drying effect, one evaluated the effects of RO surface coating process conditions on the water permeation and salt rejection properties [7]. Following drying at 60 °C, a decrease in water flux of around 65 % after drying was observed and hypothesized to be caused by increased interchain hydrogen-bonding in the PA layer. [7]. However, since this study was focused only on the impact of PA surface coating no further evaluation was performed regarding supporting layers. Two other studies evaluated the impact of membrane drying on ultrafiltration (UF)-like membrane [11,12]. Staude et al. observed that using PA and PSf like UF membrane, drying could be used to characterize the asymmetry of membranes, and that partial drying could lead to a loss of permeability [11]. Beerlage also observed that drying of UF membranes led to an irreversible loss of solvent permeability due to the collapse of the porous structure [12]. Morphological changes result in a decrease in solvent permeability ranging from 10 to 90 % of the original value due to alterations in pore size distribution and overall shrinkage of the membrane surface [12]. During UF membranes drying, structure can collapse due to the large capillary force of the pores.

To manage the impact of drying, mostly at laboratory scale, high solvent (like alcohol) treatments have been identified as efficient methods to restore the physical and morphological membrane properties partly or fully [13]. Enhancement in water permeabilities were also observed following post-treatment and attributed to the swelling of the PA film with alcohol and changes in polarity of the water-alcohol system [2]. Short (i.e., 5 min) ethanol-soaking after drying allowed to restore the initial membrane flux [13]. Despite these initial studies, significant gaps persist in understanding the effects of drying on membranes, particularly regarding their relative impact of the various layers. Moreover, it remains unclear how drying, and its potential recovery are impacting both PSf and PA layers. This is a critical issue, as the structural integrity of both the PSf and PA layers plays a pivotal role in determining the long-term performance and lifespan of membranes, as well as their suitability for recycling [14,15]. Membrane recycling, an innovative strategy to extend the lifecycle of RO membranes by repurposing them for alternative applications, faces significant challenges due to the high risk of membrane drying during storage, handling, or repurposing. As part of the membrane recycling strategies, membrane regeneration (as RO membranes) as well as membrane transformation into UF and NF (by removing PA layer) are promising strategies allowing to reuse entire modules. In this context, analyzing how drying may impact PSf and PA layers is of crucial interest.

Existing state of the art and practices demonstrated that membrane drying is a well-known concern that is to be avoided for proper operation, storage and further reuse but lacks proper assessment. By addressing this, a critical gap in current research have been observed and through a systematic approach, this study aims to gain deeper insight into the impact of drying on TFC membrane layers. A protocol was established to evaluate the drying effects on both RO and NF commercial membranes, when tested with different soaking solvents, drying and rehydration times, and reversibility over several cycles. The defined protocol was applied on TFC membranes after removal of the PA layer to dissociate the specific impact respectively on PA and PSf layers. Both permeability and rejection tests, as well as surface and bulk characterization of the membranes, were conducted.

2. Materials and methodology

2.1. Materials

2.1.1. Membranes

Commercial SW30HRLE, BW30, NF90 and NF270 membranes rolls, referred to as SW30, BW30, NF90 and NF270 from this point onward, were purchased from DWS Octochem, DuPont (Vandalia, Illinois, USA). Two different types of RO membranes (SW30 and BW30) were selected for their distinct applications and configurations. SW30 offers high salt rejection and operates at high pressures, up to 70 bar, and BW30, which provides higher permeate flow and operates at lower pressures up to 20 bar. Both SW30 and BW30 membranes, along with NF90, are fully aromatic *m*-phenylenediamine (MPD) membranes. In contrast, NF270 features a semi-aromatic piperazine-based PA layer [16–18]. All membranes were delivered in their preserving solution and cut into coupons with a surface area of 0.014 m^2 and stored at 4 °C in distilled (DI) water.

2.1.2. Chemicals

Sodium chloride (NaCl), sodium bisulfite ($NaHSO_3$), ethanol (C_2H_6O, 96 % ethanol) and sodium hypochlorite (NaClO) were purchased from Sigma Aldrich (Spain). Sodium chloride (saline water), sodium bisulfite, ethanol and DI were chosen for their varying surface tension, ranging from a lower surface tension (ethanol) to a higher surface tension (saline water). DI water and bisulfite were selected due to their common use in the water industry.

2.2. Samples preparation, drying and membrane testing protocols

2.2.1. Drying and rehydration sequences

As a baseline, a similar protocol as the one used in [13] was applied (membranes placed at 60 °C after solvent soaking) but adapted to consider several operational parameters and different solvents. Drying temperature of 60 °C allows for controlled accelerated drying procedure. Tests were later on performed also at room temperature (20 °C) during 24 h to validate observed trends in conditions closer to industrial conditions. The following parameters were assessed during the initial phase: (1) membranes were tested using different soaking solvents to evaluate their impact on drying, (2) then the impact of drying times was assessed and (3) the recovery through post-drying soaking time in ethanol was tested to determine the optimal condition for partially or fully recovering initial membrane performance. Fig. 1 shows the drying and rewetting protocols applied for all the membranes used in this study. New membranes were used in this study to focus exclusively on the drying effect, avoiding other factors related to previous membrane usage, such as compaction or fouling, that could interfere with the results and create uncertainty about the actual impact of drying. This protocol was also subsequently applied to SW30 and BW30 membranes with previously removed PA layer (named no-PA form now on) to evaluate the specific impact of drying on the PSf layer.

Initial tests were conducted with SW30 membrane to determine the optimal protocol. After initial permeability and rejection characterization, each coupon of SW30 was immersed for 1 h in different solvents including 96 % ethanol (surface tension of 22 $mN{\cdot}m^{-1}$), 1 $g{\cdot}L^{-1}$ sodium bisulfite (surface tension of 72 $mN{\cdot}m^{-1}$), DI water (surface tension of 72 $mN{\cdot}m^{-1}$), and a 70 $g{\cdot}L^{-1}$ NaCl solution (surface tension of 77 $mN{\cdot}m^{-1}$). The solvents were chosen given their distinct surface tensions and their potential presence in discharged modules: DI water and 70 $g{\cdot}L^{-1}$ mimic permeate and brine from desalination plants; sodium bisulfite is commonly used as preservative and biocide and ethanol is recommended in case of membrane drying. Subsequently, membranes were superficially rinsed with DI to remove residual solvent, dried for 1 h in an oven (Memmert) at 60 °C (same temperature used in previous study

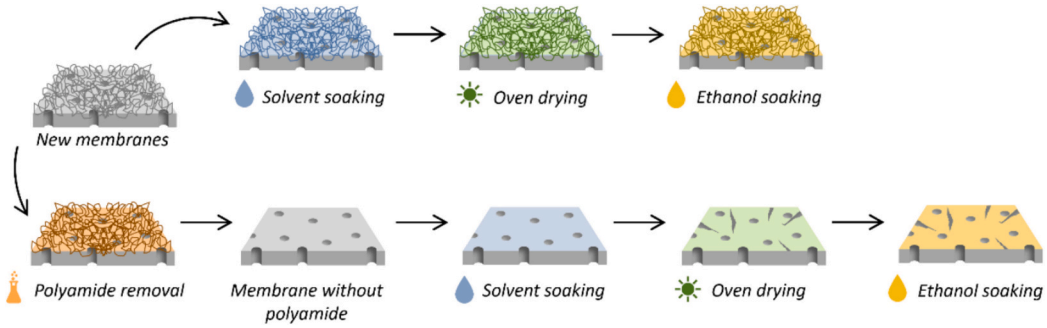

Fig. 1. Drying and rewetting protocols applied for all the membranes used in this study.

[13]) and characterized to assess the impact of drying and solvent used on permeability and salt rejection performance. Then, all coupons were immersed in 96 % ethanol for 1 h to evaluate potential rehydration before final characterization was conducted. Additional tests were carried out using SW30 membrane to evaluate various drying time including 15 min, 1 and 4 h. In addition, 4 contact times with 96 % ethanol for rehydration were tested (1, 5, 30, and 60 min).

Then, the optimized procedure was applied to BW30, NF90, and NF270 membranes, i.e. (1) the coupons were initially soaked in 96 % ethanol, (2) dried for 1 h at 60 °C, and (3) rehydrated by soaking them again in 96 % ethanol.

To assess the impact of drying temperature, additional tests were performed on SW30 and BW30 membranes, both with and without the PA layer. First, the membranes were soaked in 96 % ethanol for 1 h, then dried at room temperature (20 °C) for 24 h. Following this period, the membranes were re-soaked in 96 % ethanol to rehydrate them.

2.2.2. Membrane conversion - PA layer removal

To specifically assess the relative impact of the drying process on the PA layer and the PSf layer, the PA layer was removed by chemical oxidation by applying a 300,000 ppm·h dose free chlorine treatment as explained in the literature to convert RO to UF membranes [14,15]. Full removal of the PA layer was confirmed through Field-Emission Scanning Electron Microscope (FE-SEM) and Fourier Transform Infrared (FTIR) characterization. Subsequently, the established protocol (as in 2.2.1) was applied to the no-PA SW30 and BW30 layer membranes to evaluate the impact of drying and rehydration on the PSf layer.

2.3. Permeability and rejection set-up

A high-pressure lab-scale filtration set-up was used to characterize membranes at 15 bar with a 2 $g{\cdot}L^{-1}$ sodium chloride feed solution. 20 L feed solution was maintained at 20 °C ± 0.5 °C in a tank (SETPAR export, Spain) and circulated via a high-pressure pump (CATpumps piston pump model 3CP1231, USA) at 2 $L{\cdot}min^{-1}$ to a Sepa CFX Cell (Sterlitech, USA). The feed pressure was regulated using a back-pressure valve on the retentate line and the permeate solution was sent back to the feed tank. Permeate flux was measured by mass change over time using a Kern PCB 6000–1 balance. Samples were collected every 10 min for conductivity measurement with a Crison Instruments meter and returned to the permeate tank. Weight and pressure data were continuously recorded with a Bluetooth-based Arduino system.

The permeability (J) was calculated using Eq. 1. ΔV being the permeated volume (L), A the effective membrane filtration area (m^2), Δt the time between samples (h) and ΔP the transmembrane pressure (bar) as per Eq. 1.

$$J = \frac{\Delta V}{A{\cdot}\Delta t{\cdot}\Delta P}\left[\frac{L}{m^2{\cdot}h{\cdot}bar}\right] \quad (1)$$

A temperature correction factor (TCF) was applied to normalize the value of permeability at 25 °C, in accordance with the DuPont manual [6]. The rejection coefficients (%R), in this case sodium chloride rejection was determined by Eq. 2. C_o is the conductivity of the feed and C_f is the conductivity of the permeate.

$$\%R = \left(1 - \frac{C_o}{C_f}\right)[\%] \quad (2)$$

2.4. Membrane surface characterization

2.4.1. Water contact angle

Contact angle measurements were conducted using the sessile drop method with an Attention Theta instrument from Biolin Scientific. A 4 μL solvent drop was carefully dispensed onto the membrane surface using a syringe. The software automatically generated tangent lines to both sides of the drop and calculated the average contact angle. Each measurement lasted for 20 s and was repeated 10 times per sample. Contact angle was used to determine the hydrophobicity ($\theta > 90°$) and hydrophilicity ($\theta < 90°$) of membrane surface using drops of water.

2.4.2. ATR-FTIR

FTIR spectroscopy analysis was conducted using a PerkinElmer Spectrum 100 FT-IR instrument equipped with a 45° multi-reflection ZnSe flat plate crystal as the Attenuated Total Reflectance (ATR) element. Spectra were acquired within the range of 650–4000 cm^{-1} at a resolution of 4 cm^{-1}. Each sample underwent analysis three times to ascertain the standard deviation. ATR-FTIR was used to identify PA degradation after membrane conversion and to evaluate if drying or rehydration has an impact on the PA composition. The FTIR analysis was focused on the primary bands representative of PSf and PA layers, such as aliphatic alcohols (1040 cm^{-1}), amide II (1550 cm^{-1}), amide I (1,650 cm^{-1}) and N-H + O-H bonds (3300 cm^{-1}) [19,20].

2.4.3. FE-SEM

FE-SEM membrane surface analysis was conducted using a NanoSEM 230 instrument. The samples were air-dried prior to placing on the sample holder. For each experiment, a rectangular piece of the sample was prepared and subsequently coated with a 15 nm layer of carbon via sputter coating. Imaging was conducted using an accelerating voltage of 5 kV in backscattered electron detection mode and a working distance between 6 and 7 cm.

2.4.4. Liquid-liquid perm-porometry

Pore feature analysis, involving evaluation of average pore size, pore size range, and distribution, was executed utilizing the INNOVA 500 liquid-liquid porometer, manufactured by Poretech Instruments INC, Taiwan.

2.4.5. Laser profilometry

Surface roughness and surface profile data were acquired through the utilization of the LEXT OLS4100 3D laser microscope, produced by Olympus, Australia. This equipment employs laser scanning to conduct

non-contact 3D measurements of intricate surface features.

3. Results and discussion

3.1. Initial assessment of drying and rehydration conditions

The protocol was initially tested using SW30 membrane to define the optimal operating conditions. The impacts of soaking solvents, drying durations, and rehydration periods were assessed.

3.1.1. Impact of soaking solvents

Membrane permeabilities and rejection were assessed at each step of the drying-rehydration protocol using four different solvents as shown on Fig. 2a. After drying, a severe decrease in permeability and salt rejection was observed after soaking in all tested solvents, followed by a high recovery during the rehydration phase. The most significant permeability decreases after 1 h of drying at 60 °C was observed for the coupon previously soaked in 96 % ethanol, with a permeability reduction of approximately 70 %, while the least affected was the one soaked in a saline solution (7 % *w/v* NaCl), showing a limited decrease of 9 %. This discrepancy can be correlated to the surface tension of the tested solvents. Ethanol has a significantly lower surface tension compared to saline water, i.e., 22 and 77 $mN{\cdot}m^{-1}$ respectively, at 20 °C.The presence of salt in the saline solution helps retain moisture within the membrane pores, mitigating the drying impact. Coupons soaked in sodium bisulfite and DI water (surface tension of 72 $mN.m^{-1}$), also experienced permeability decrease (approximately 40 %) but to a lower extent than for ethanol. Post-rehydration, all membranes reached a permeability around 2.3 $L{\cdot}m^{-2}{\cdot}h^{-1}{\cdot}bar^{-1}$, recovering to their initial value of 2.3 $L{\cdot}m^{-2}{\cdot}h^{-1}{\cdot}bar^{-1}$ and demonstrating reversibility of the drying process. After rehydration, salt rejection was partly/fully recovered (Fig. 2a); only for membrane soaked in saline water a different trend that could be hypothesized to result from leaching of some remaining salt from previous saline water soaking. The results obtained are consistent with those reported in [13], where SW30 coupons initially soaked in ethanol for 1 h and then dried exhibited a permeability decrease of approximately 65 %. However, upon re-wetting the dried coupons in ethanol, the initial permeability was fully restored. This behavior was attributed to one main factor: impaired membrane-water interactions, where intermolecular water-polymer hydrogen bonds were likely replaced by interchain hydrogen bonds during the drying process [13].

3.1.2. Drying time

Different drying times from 15 min to 4 h were applied to the SW30 membrane to further assess drying intensity on permeability. Fig. 2 illustrates the permeability (b) and salt rejection (c) changes for each solvent across the different drying times. Permeability decrease with time for all solvents was observed, but with very distinct patterns. In the case of ethanol, 15 min drying proved to have already a very severe effect with a decrease in permeability of 68 %, followed by a plateau, indicating that a steady state was reached, i.e., membrane fully dried. With other solvents, permeability loss was observed over the 4 h, indicating a slower drying impact. During the initial 15 min, permeability decreased by 31 % for DI water, 31 % for bisulfite, and 22 % for saline water. After 4 h, DI water and bisulfite showed more severe permeability losses of 73 and 82 %, respectively but still to a lesser extent than the ethanol-soaked coupon featuring the highest permeability loss at 86 %. Saline water was the least affected by drying, with a final permeability loss of only 37 % after 4 h. The loss of permeability can be connected to the drying intensity and kinetic which is directly connected to solvents surface tension. Using saline water as solvent allowed to mitigate drying effect due to its higher surface tension and as such demonstrated that storing membranes in saline water may help for their preservation.

High variability was observed with regards to salt rejection (Fig. 2c), however general trends show that a decrease is observed for all membranes following drying most likely resulting from the water permeability decrease.

3.1.3. Rehydration time

Rehydration performance using 96 % ethanol was applied on previously dried membranes. Contact times of 1, 5, 30 and 60 min were tested, permeability and salt rejection are shown in Fig. 2d. Initial values correspond to membranes dried for 1 h at 60 °C using 96 % ethanol as solvent. Soaking the membrane in ethanol for 1 min already nearly restored permeability to its initial value, reaching 2.2 $L{\cdot}m^{-2}{\cdot}h^{-1}{\cdot}bar^{-1}$, compared to the original value of 2.3 $L{\cdot}m^{-2}{\cdot}h^{-1}{\cdot}bar^{-1}$. Longer soaking time, up to 1 h, did not show any further improvement. Salt rejection followed a similar pattern, reaching 97 % after 5 min of soaking in ethanol. Those results confirm the potential to use ethanol for full and quick recovery of initial characteristics of PA selective layer of dried membranes.

3.1.4. Drying-rehydration cycles

A SW30 coupon underwent multiple cycles of drying and rehydration (Fig. 2e) to assess membrane behavior after each cycle. As previously observed, during the first cycle, the permeability decreased by around 54 % after drying but was recovered upon rehydration, nearly reaching its initial value. This pattern was consistent along multiple cycles of drying and rehydration, with similar values achieved each time. Consequently, it can be concluded that the membrane can undergo multiple drying cycles without performance deterioration and that PA layer can consistently be restored back by soaking in ethanol. As reported in [13], it is expected that intermolecular water-polymer bonds were replaced by interchain hydrogen bonds and that the ethanol soaking allowed to revert back the process.

3.2. Comparison of NF and RO membranes

3.2.1. Permeability and salt rejection tests

Permeabilities and salt rejections of each membrane tested during the three different stages (initial, post-drying and post-rehydration) are presented in Fig. 3. BW30 and NF90 presented similar behaviors than SW30 membrane with a severe permeability decrease after drying, followed by partial recovery upon rehydration, with no significant impact on salt rejection. BW30 membranes presented a permeability decrease of 66 % after drying and a partial recovery of 76 % post-rehydration. As observed for SW30 and BW30 membranes, drying on NF90 membrane has a notable impact on permeability, leading to 84 % decrease on permeability. After rehydration, limited permeability recovery of 41 % was observed. Differences between tested membranes can also be attributed to the slightly different type of PA layer composition as reported in the literature, showing differences between coated and uncoated membranes with polyvinyl alcohol (PVA) [21,22]. NF270 presented similar behavior in terms of water permeability with a decrease of 48 % after drying and almost full recovery after soaking in ethanol. However, salt rejection further decreased after rehydration. The irreversibility of the process demonstrated a permanent modification of the active layer which could relate to its distinct nature, i.e., NF270 features a semi-aromatic piperazine-based PA layer. Also, NF membranes are highly sensitive to temperature, i.e., especially NF270 might have a limited use when the water temperature exceeds 45–50 °C [18]. Thus, the drying procedure at 60 °C used might have altered the polymeric structure of the membrane.

3.2.2. Surface characterization

Contact angle measurements at each stage (initial, dried and rehydrated) for RO and NF90 membranes did not show a significant trend, with the values obtained here different from those observed the literature [23–25]. However, on NF270 membranes significant variation on contact angle were observed, probably due to the different chemical composition from the semi-aromatic PA layer. NF270 showed a contact angle increasing from an initial value of 17° to 44° after rehydration.

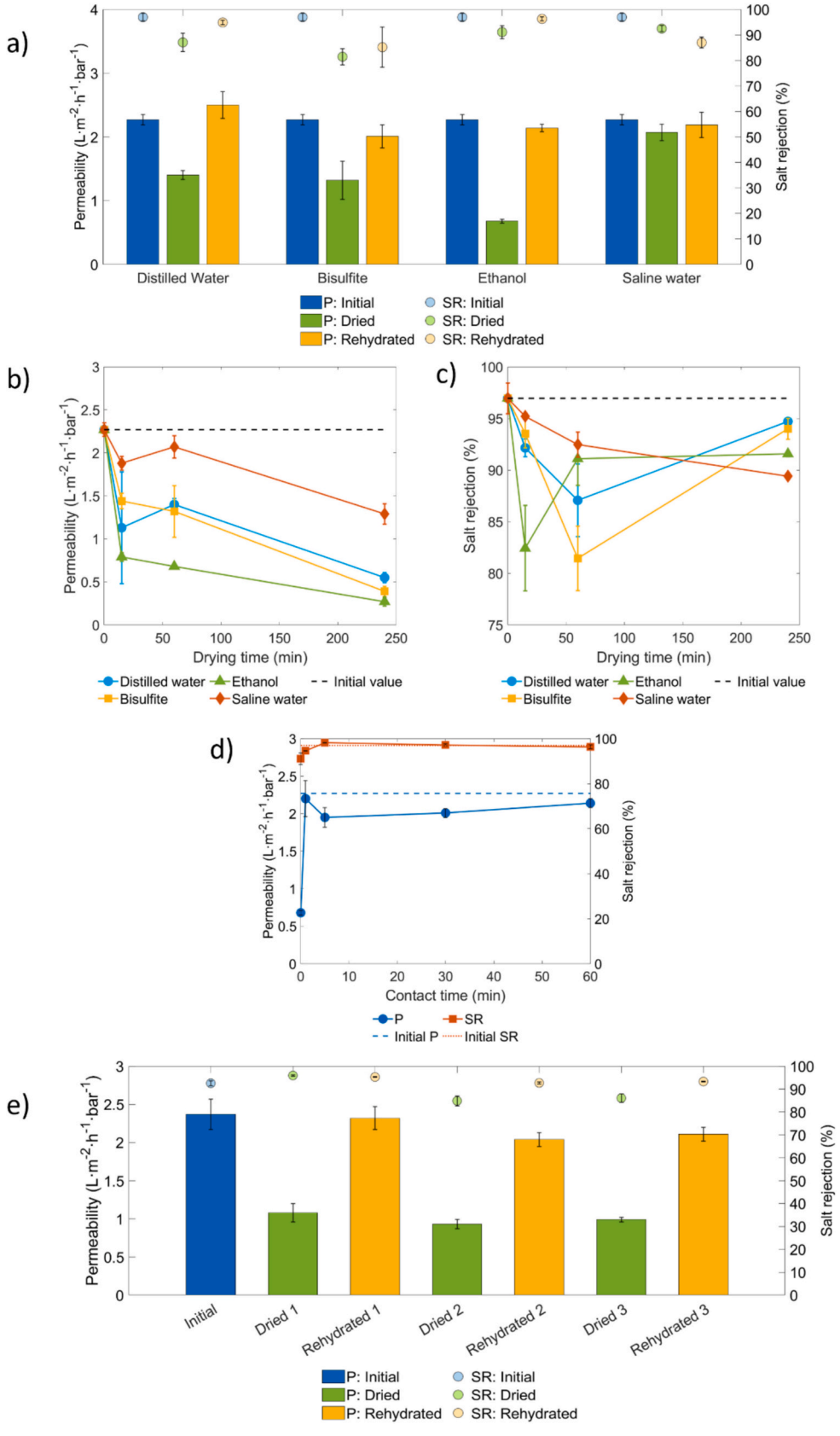

(caption on next page)

Fig. 2. **a)** Permeability and salt rejection of SW30 after 1 h soaking in various solvents at each stage of the drying-rehydration protocol (initial - blue, post-drying - green and post-rehydration - yellow). **b and c)** Impact of drying times on permeability (b) and salt rejection (c) of SW30 after 1 h soaking in different solvents. **d)** Impact of rehydration time (soaking in ethanol) on permeability and salt rejection of SW30. The initial permeability (stripped blue line) and salt rejection (dot red line) of SW30 membrane were shown. **e)** Multiple drying-rehydration cycle permeabilities and salt rejection for SW30 membrane during the different stages (initial - blue, post-drying - green and post-rehydration - yellow). (For interpretation of the references to colour in this figure legend, the reader is referred to the web version of this article.)

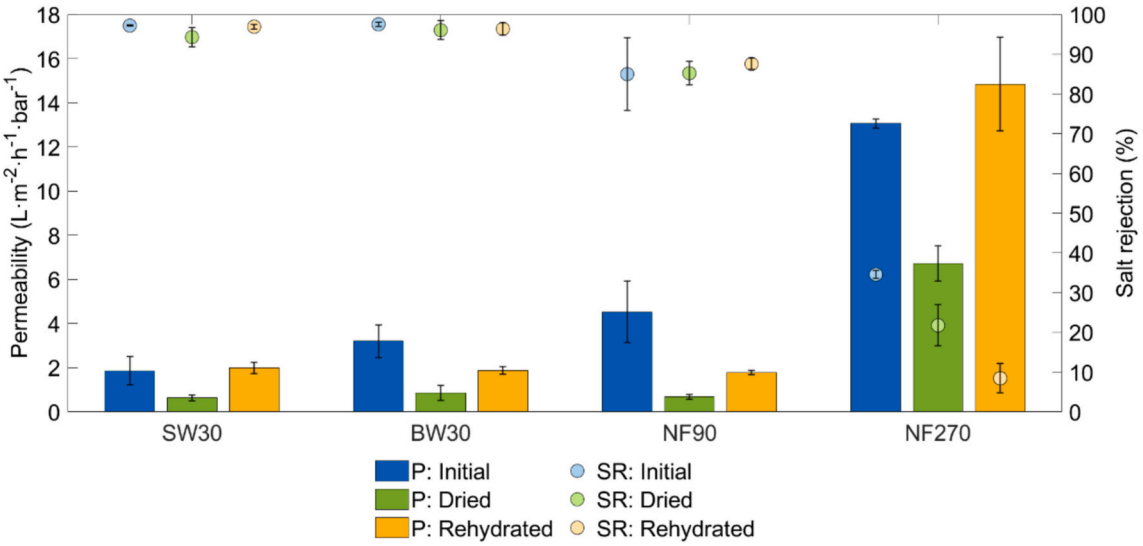

Fig. 3. Permeability and salt rejection of each membrane (SW30, BW30, NF90 and NF270) during the different stages (initial - blue, post-drying - green and post-rehydration - yellow). (For interpretation of the references to colour in this figure legend, the reader is referred to the web version of this article.)

NF270 typically contains a higher quantity of functional groups that readily dissociate upon contact with ethanol, increasing its hydrophobicity evidenced by a higher contact angle. These changes on membrane surface functional groups may explain observed decreasing salt rejection (Fig. 3).

No significant changes in FE-SEM analysis were observed post-drying and rehydration as shown on Fig. 4 (SW30: a, b and c and BW30: g, h and i) showing similar ridge-and-valley structures during the different stages.

3.3. Performance of membranes without PA layer

3.3.1. Permeability and salt rejection tests

The SW30 and BW30 membranes underwent chlorine treatment to remove the PA layer, converting them into UF-like membranes. Membranes were then processed through the same drying and rehydration protocol and were characterized after each step. Fig. 5a illustrates their permeabilities and salt rejections. Upon removal of the PA layer, the permeability of both membranes increased up to 275 $L{\cdot}m^{-2}{\cdot}h^{-1}{\cdot}bar^{-1}$, similar value than what observed for typical UF membranes [26]. Also, as expected, a significant drop in salt rejection was observed, down to below 10 % for both tested membranes.

After drying, the permeability of both membranes exhibited a sharp decline, dropping down to 26 $L{\cdot}m^{-2}{\cdot}h^{-1}{\cdot}bar^{-1}$ for no-PA-SW30 and 20 $L{\cdot}m^{-2}{\cdot}h^{-1}{\cdot}bar^{-1}$ for no-PA-BW30, with reductions of 91 and 93 %, respectively. Those results are in line with past study [12], which reported an irreversible morphology change by a decrease in pore size distribution and overall membrane surface shrinkage, when PSf UF membranes were subjected to a drying process.

After rehydration, a 30 % recovery in permeability was observed for the no-PA-SW30 membrane, remaining significantly below initial values. For the no-PA-BW30 membrane, the permeability after rehydration was not at all recovered. Compared to initial values of permeability of 275 $L{\cdot}m^{-2}{\cdot}h^{-1}{\cdot}bar^{-1}$, the no-PA-SW30 and no-PA-BW30 membranes exhibited respectively an 86 and 95 % reduction in permeability after rehydration, showing a permanent impact on membrane performance. However, despite the limited recovery of permeability after rehydration, the PSf layer alone consistently demonstrates higher permeability than the membrane with the PA layer intact. As a result, the impact of factors such as drying, rehydration, and long-term stability on the PSf layer may not receive the attention they warrant, even though they play a crucial role in the membrane's overall behavior. Such an issue is of critical importance especially for EoL membrane transformation when PA layer is removed since the PSf support layer likely undergoes permanent damage from the first drying cycle, showing no signs of recovery regardless of subsequent treatments. However, and as shown in Fig. 2e, as long as the PA layer membrane remains, the effects of drying are hidden and may appear reversible after ethanol-soaking not affecting permanently permeability and flux of the membrane.

3.3.2. Surface characterization

Following the RO-to-UF conversion process, the membrane became less hydrophilic compared to those with the PA layer (Fig. 4b), as indicated by an increase in the contact angle by 29 and 36 % for the no-PA-SW30 and BW30 membranes, respectively. Once the PA layer was removed, the measured contact angles were approximately 65°, as shown in Fig. 4b. This value closely corresponds to the contact angle of PSf previously reported [27], which suggests that the PA layer have been removed after the chlorine treatment. The PA layer removal was also confirmed through FTIR analysis, serving as a semi-quantitative method. Notably, a reduction of approximately 70 % in both amide I (1,650 cm^{-1}) and amide II (1550 cm^{-1}) bands was observed (Fig. 5c), when comparing initial membranes with those without PA layer. Additionally, a decline between 74 and 88 % for the no-PA-SW30 and the BW30 membranes for the peak at 3300 cm^{-1} has been noted respectively, confirming the influence of the PA layer on this peak.

Fig. 4 reports FE-SEM images of these membranes at various stages (initial, dried, and rehydrated). They confirmed an almost full removal of the PA layer with an elimination of the typical ridge-and-valley

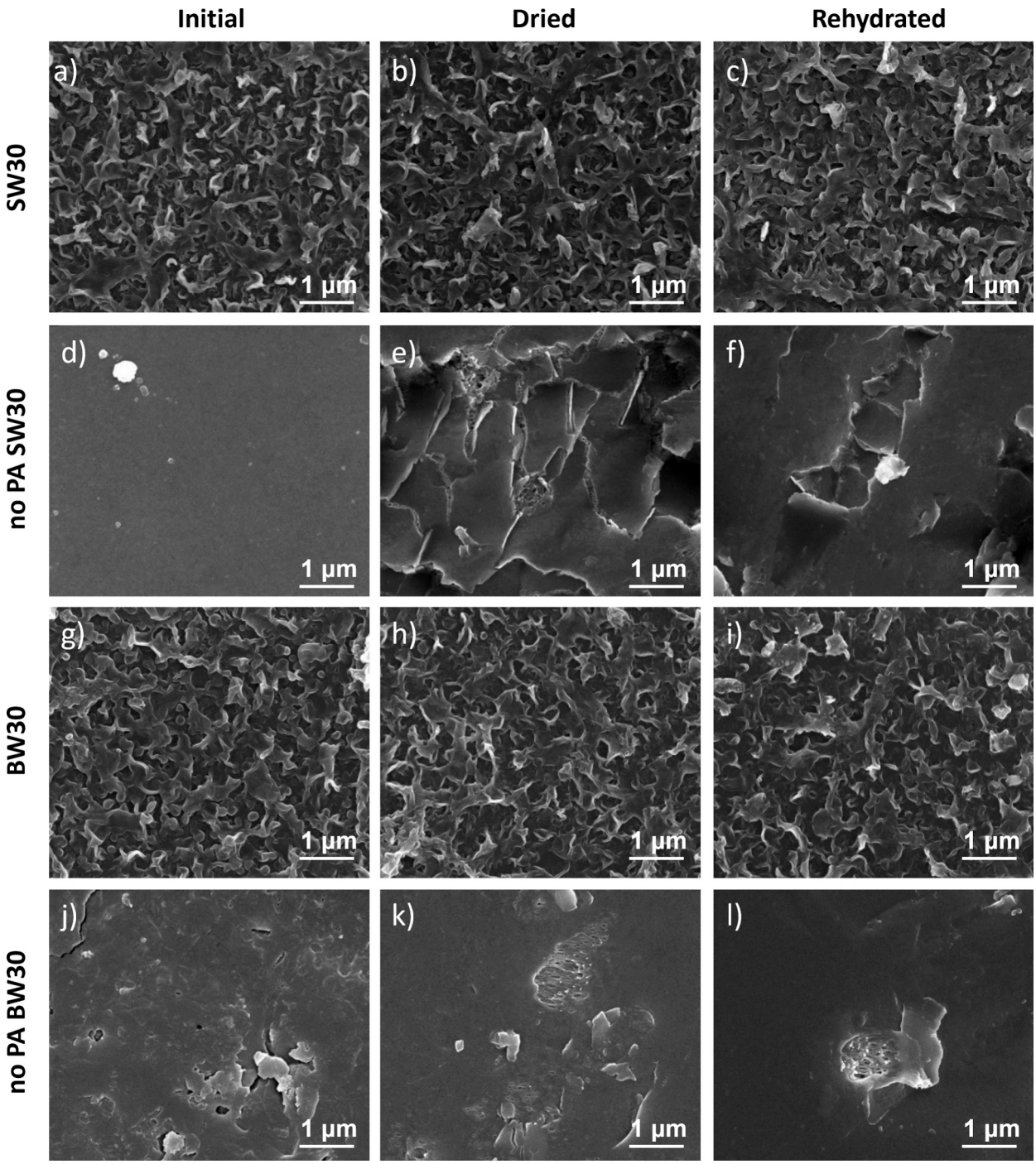

Fig. 4. FE-SEM images for the SW30 (a- initial, b- dried, c- rehydrated), no-PA-SW30 (d- initial, e- dried, f- rehydrated), BW30 (g- initial, h -dried, i- rehydrated) and no-PA-BW30 (j- initial, k- dried, l- rehydrated).

structure of the PA layer, as observed in Figs. 4 a and g, into a few residual PA remnants on the smooth PSf surface layer as shown in Figs. 4 d and j. These findings confirm that the PA layer was almost completely removed, resulting in permeabilities comparable to those reported for UF-like membranes in the literature. [14].

Alterations on PSf layer after drying were observed (Figs. 4 e and k) with the appearance of cracks. Even after rehydration, the breaks on the membrane surface appeared in all cases, as illustrated in Figs. 4 f and l, suggesting a permanent impact that cannot be restored by ethanol treatment. Cracks were not observed in previous studies [15] that explored the transformation of RO membranes into UF-like membranes, suggesting that their appearance is unrelated to the chlorine treatment used to remove the PA layer but is resulting from the drying protocol. These results underscore the permanent damage incurred on the PSf layer demonstrating that drying impacts not only the PA layer, but also the PSf layer which is typically not considered since RO membranes performances are typically assessed through permeability tests which are evaluating the potential degradation of the PA layer. The results obtained regarding the impact on the PSf layer after drying significantly differed from those reported in a previous study which suggested that all morphological changes affecting membrane performance occurred in the PA layer [13]. However, our findings align with those from research on PSf UF membranes [12], presenting substantial evidence that drying induces permanent changes in the PSf layer. Recognizing and addressing

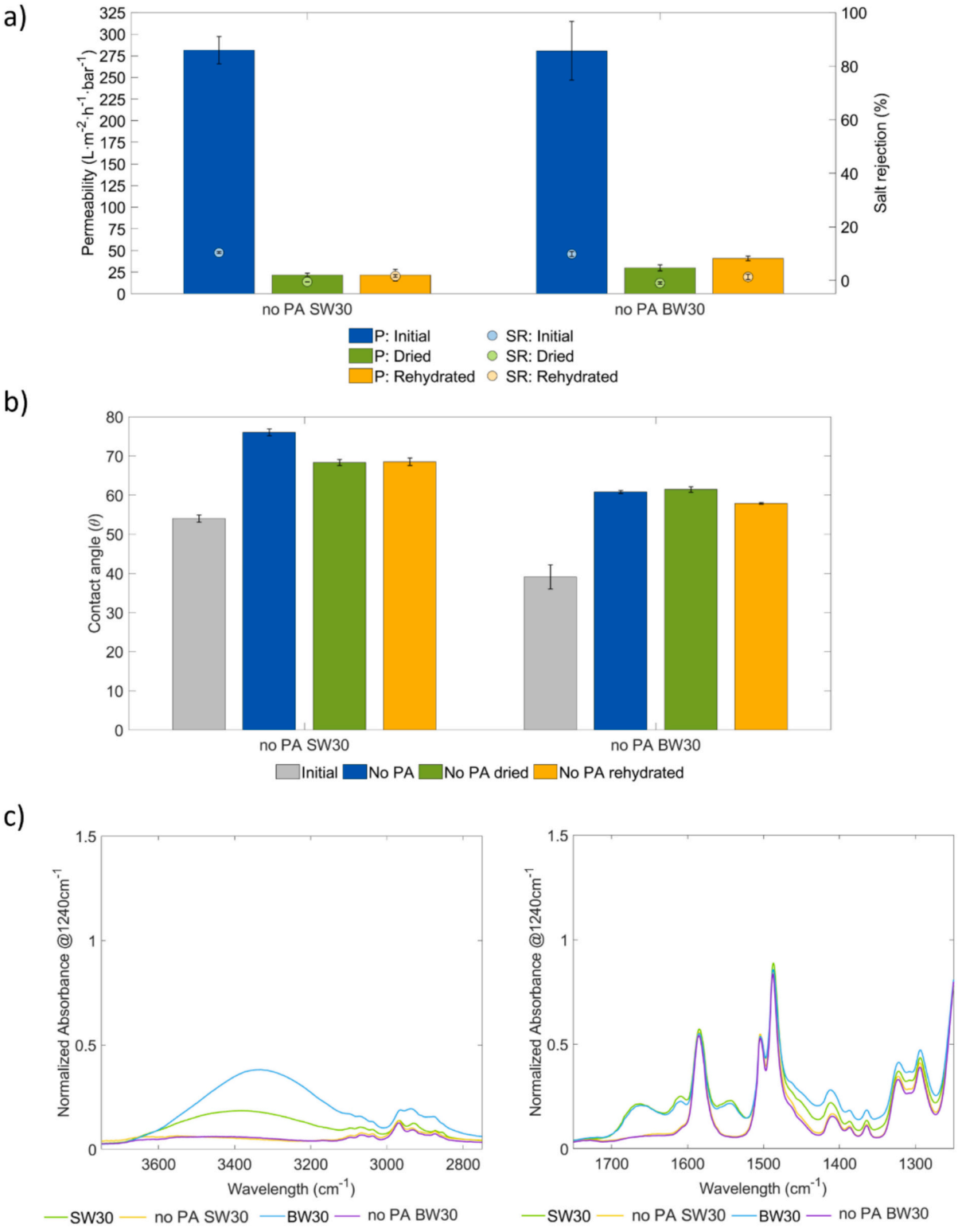

Fig. 5. a) Permeability and salt rejection of each no-PA membrane (SW30 and BW30) during the different stages (initial - blue, post-drying - green and post-rehydration - yellow). **b)** Contact angle for both membranes before and after removing the PA layer and for dried and rehydrated states without the PA layer. **c and d)** FTIR spectra for the studied membranes (SW30 - green, no-PA-SW30 - yellow, BW30 - blue and no-PA-BW30 - purple). (For interpretation of the references to colour in this figure legend, the reader is referred to the web version of this article.)

these effects is crucial for advancing membrane technology and improving strategies for proper membrane management and especially in the case of end-of life membrane recycling and transformation were the PSf layer properties becomes primordial [28–30].

Additionally, laser profilometry and liquid-liquid perm-porometry were conducted on specific samples to assess the potential changes in roughness and ultimate perforation of the materials if severely damaged. Laser profilometry was selected to evaluate roughness at large scale since it allows for roughness evaluations down to 1000 nm on X-Y and 10 nm on Z, while being non-contact and therefore not suffering from

the same scaling issues as AFM. On the other hand, liquid-liquid perm-porometry was performed on multiple samples with and without PA layer to evaluate irreversible loss of integrity following drying the PSf layer. Tests were conducted on RO membranes without PA layer (supplementary information, Figs. S1 and S2). Through profilometry (Fig. S1), which is particularly effective for assessing large-scale surface features with high accuracy, heterogeneity was observed on samples but without clear correlation to drying impact. Liquid-liquid perm-porometry performed on SW30 membrane (Fig. S2), confirmed the loss of permeability tests observed earlier attributed to the support pore size collapse. However, pore size distribution did not allow to draw a clear trend with regards to pore collapsing probably due to small pore size measured, touching the limits of the characterization technic..

3.4. Performance of air-dried membranes versus 60 °C drying

To further assess the impact of drying conditions on membrane modifications, RO membranes were dried for 24 h at room temperature (20 °C) to evaluate whether the results obtained from oven drying at 60 °C were due to temperature-related polymer degradation.

As shown in Fig. 6, differences were observed between the two drying methods. For SW30 membranes, drying at 60 °C had a slightly greater impact, compared to ambient temperature drying, resulting in a 54 % difference. This indicates that air-dried membranes did not achieve the same fully dried state as those dried at 60 °C due to the slower kinetic for solvent evaporation at lower temperature. However, after the rehydration stage, the SW30 membrane showed a higher permeability compared to the initial one suggesting than the initial membrane may have suffered from partial drying during storage before starting the experiment. In contrast, for BW30 membranes, the air-dried coupons exhibited a similar permeability relation between initial and dried membranes than the one dried at 60 °C. Rehydration process allowed nearly full recover initial permeabilities conditions for both coupons regardless of the drying conditions.

Membranes without a PA layer also exhibited a decrease in permeability, following ambient temperature-drying or drying at 60 °C. The no-PA-SW30 membrane demonstrated a slight reduction, consistent with the hypothesis that the initial membrane coupon was partially dried prior to the experiments. After rehydration, the membrane was unable to recover its initial permeability, indicating a permanent impact of drying, irrespective of the temperature. In contrast, the no-PA-BW30 membrane experienced a more significant reduction in permeability compared to the no-PA-SW30, with the drying at 60 °C causing the greatest impact. Nevertheless, after rehydration, both membranes exhibited lower permeability than their initial values. Regarding the values obtained, and as discussed in Section 3.3, after the rehydration stage, membranes without the PA layer were unable to recover their initial state, with permeabilities of 40 $L{\cdot}m^{-2}{\cdot}h^{-1}{\cdot}bar^{-1}$ for both no-PA membranes and both drying methods. This confirms the permanent impact that drying has on the PSf layer, regardless of the drying temperature.

These findings suggest that, although drying at 60 °C appears to have a greater initial impact than drying at room temperature, the presence of cracks, as observed in Fig. 5e and k, cannot be attributed solely to the higher temperature but rather to the drying process itself since it has been also observed on samples dried at room temperature.

4. Conclusions

In this study, the impact of drying and rehydration of RO and NF membranes has been systematically assessed. For all tested membranes, the drying process impacted the membrane performance by decreasing permeability and salt rejection. Rate of drying was linked to the surface tension of the solvent present within the membrane. The previous soaking of membranes in solvents like saline water proved to slow down the drying process and therefore may be of interest for membrane storage. Specific analyses of PA and PSf layers demonstrated that the PA layer is affected by drying but can be partial or fully recovered after soaking the membrane in ethanol. Drying of the PSf layer had a permanent impact with a loss of permeability and provoking cracks on the surface which cannot be reverted by soaking the membrane in ethanol. The impact on the permeability of the PSf layer is generally hindered by the PA layer characterization, which is the limiting factor for permeability/rejection tests. This study demonstrated that avoiding drying is crucial for extending the lifecycle of RO membranes and enabling their effective recycling. Drying can degrade their structural integrity and performance, making them unsuitable for reuse. Proper storage and handling after use are essential to being able to recycle the membranes and move towards a sustainable water treatment practices. Further work should include advanced surface and molecular-level characterizations, such as polymer chain dynamics and solvent–polymer interactions, to gain deeper insight into the fundamental mechanisms involved in

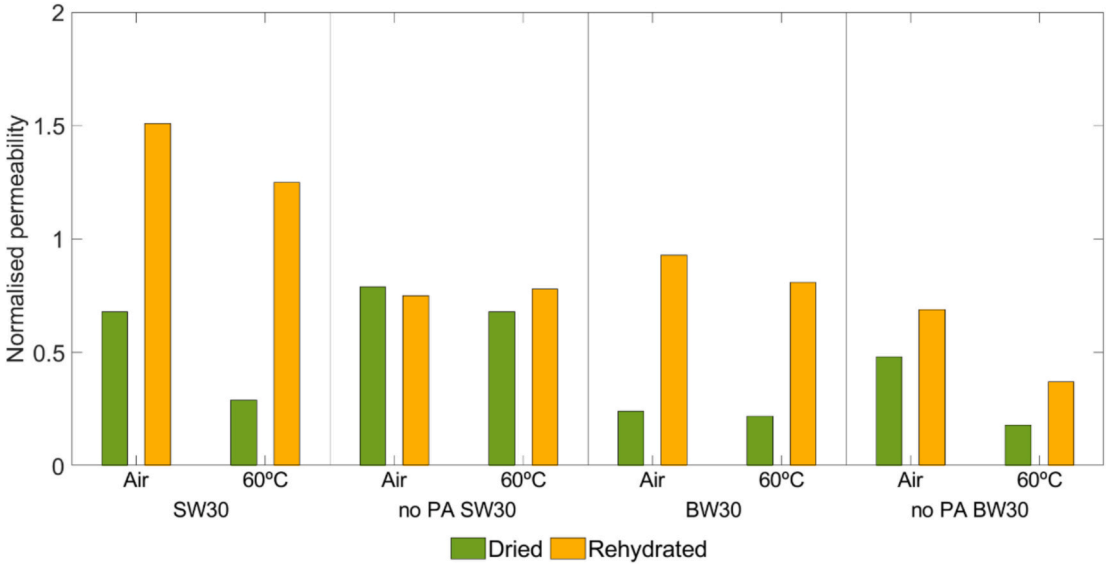

Fig. 6. Normalised permeability for the air-dried and 60 °C oven dried membranes in the different stages (dried – green and rehydrated – yellow) versus initial membrane permeability. (For interpretation of the references to colour in this figure legend, the reader is referred to the web version of this article.)

membrane behavior during drying. Furthermore, studies focusing on additional drying temperature gradients presence of fouling, evaluation at membrane module scale and cost evaluation should be carried out to better understand drying impact under real operation conditions.

CRediT authorship contribution statement

Bianca Zappulla-Sabio: Writing – original draft, Methodology, Investigation, Data curation. **Pierre Le-Clech:** Writing – review & editing, Supervision. **Ludovic F. Dumée:** Writing – review & editing, Supervision. **Hari Kalathil Balakrishnan:** Data curation, Formal analysis. **Hèctor Monclús:** Writing – review & editing, Supervision. **Gaëtan Blandin:** Writing – review & editing, Validation, Supervision, Project administration, Methodology, Funding acquisition.

Declaration of competing interest

The authors declare the following financial interests/personal relationships which may be considered as potential competing interests: Gaëtan Blandin has been an executive guess editor of Special Issue of the Journal of Water Process Engineering. He was not involved with neither the review process nor the handling of paper. Ludovic F. DUMEE has been an editor of the Journal of Water Process Engineering since July 2019. He was not involved with neither the review process nor the handling of paper. If there are other authors, they declare that they have no known competing financial interests or personal relationships that could have appeared to influence the work reported in this paper.

Acknowledgments

This work is part of the project OSMO4LIVES (PID2021-127629OA-I00) funded by MICIU/AEI/10.13039/501100011033 and EDRF/EU. Bianca Zappulla received the support of a FI-SDUR predoctoral aid program of the Department of Research and Universities of the *Generalitat de Catalunya* (AGAUR) [REF: 2023 FISDU 00267]. Gaetan Blandin received the support of a fellowship from "la Caixa" Foundation (ID 100010434) [REF: LCF/BQ/PR21/11840009] and acknowledges the Ramon y Cajal Research Fellowship RyC2022-035843-I funded by MICIU/AEI/10.13039/501100011033. Hèctor Monclús acknowledges Agencia Estatal de Investigación of the Spanish Ministry of Science, Innovation and Universities (MCIU) for partially funding this research through the Ramon y Cajal Research Fellowship (RYC2019-026434-I). LEQUiA [2021-SGR-01352] has been recognized as consolidated research group by the Catalan Government. Open Access funding provided thanks to the CRUE-CSIC agreement with *Elsevier*.

Appendix A. Supplementary data

Supplementary data to this article can be found online at https://doi.org/10.1016/j.jwpe.2025.108110.

Data availability

Data will be made available on request.

References

[1] X. Lu, M. Elimelech, Fabrication of desalination membranes by interfacial polymerization: history, current efforts, and future directions, Chem. Soc. Rev. 50 (11) (2021) 6290–6307, https://doi.org/10.1039/D0CS00502A.
[2] B. Khorshidi, B. Soltannia, T. Thundat, M. Sadrzadeh, Synthesis of thin film composite polyamide membranes: effect of monohydric and polyhydric alcohol additives in aqueous solution, J. Membr. Sci. 523 (2017) 336–345, https://doi.org/10.1016/j.memsci.2016.09.062.
[3] S. Qiu, L. Wu, L. Zhang, H. Chen, C. Gao, Preparation of reverse osmosis composite membrane with high flux by interfacial polymerization of MPD and TMC, J. Appl. Polym. Sci. 112 (4) (2009) 2066–2072, https://doi.org/10.1002/app.29639.
[4] L.F. Greenlee, D.F. Lawler, B.D. Freeman, B. Marrot, P. Moulin, Reverse osmosis desalination: water sources, technology, and today's challenges, Water Res. 43 (9) (2009) 2317–2348, https://doi.org/10.1016/j.watres.2009.03.010.
[5] B.M. Souza-Chaves, M.A. Alhussaini, V. Felix, L.K. Presson, W.Q. Betancourt, K. L. Hickenbottom, A. Achilli, Extending the life of water reuse reverse osmosis membranes using chlorination, J. Membr. Sci. 642 (2022) 119897, https://doi.org/10.1016/j.memsci.2021.119897.
[6] DuPont., February, RO NF FilmTec Manual, FilmTec™ Reverse Osmosis Membranes Technical Manual, 2023. https://www.dupont.com/content/dam/dupont/amer/us/en/water-solutions/public/documents/en/RO-NF-FilmTec-Manual-45-D01504-en.pdf.
[7] X. Feng, J. Zhu, J. Jin, Y. Wang, Y. Zhang, B. Van der Bruggen, Polymers of intrinsic microporosity for membrane-based precise separations, Prog. Mater. Sci. 144 (2024) 101285, https://doi.org/10.1016/j.pmatsci.2024.101285.
[8] P. Su, S. Chen, L. Chen, W. Li, Constructing polymer/metal-organic framework Nanohybrids to design compatible polymer-filler-polymer membranes for CO2 separation, J. Membr. Sci. 691 (2024) 122246, https://doi.org/10.1016/j.memsci.2023.122246.
[9] Z. Wang, Z. Chen, Z. Zheng, H. Liu, L. Zhu, M. Yang, Y. Chen, Nanocellulose-based membranes for highly efficient molecular separation, Chem. Eng. J. 451 (2023) 138711, https://doi.org/10.1016/j.cej.2022.138711.
[10] J. da Silva Burgal, L. Peeva, P. Marchetti, A. Livingston, Controlling molecular weight cut-off of PEEK Nanofiltration membranes using a drying method, J. Membr. Sci. 493 (2015) 524–538, https://doi.org/10.1016/j.memsci.2015.07.012.
[11] E. Staude, J. Passlack, Characterization of ultrafiltration membranes by drying, J. Membr. Sci. 28 (2) (1986) 209–223, https://doi.org/10.1016/S0376-7388(00)82211-5.
[12] M.A.M. Beerlage, Polyimide ultrafiltration membranes for non-aqueous systems. (1994), https://doi.org/10.3990/1.9789090071404.
[13] J.S. Louie, I. Pinnau, M. Reinhard, Effects of surface coating process conditions on the water permeation and salt rejection properties of composite polyamide reverse osmosis membranes, J. Membr. Sci. 367 (1) (2011) 249–255, https://doi.org/10.1016/j.memsci.2010.10.067.
[14] R. García-Pacheco, J. Landaburu-Aguirre, S. Molina, L. Rodríguez-Sáez, S.B. Teli, E. García-Calvo, Transformation of end-of-life RO membranes into NF and UF membranes: evaluation of membrane performance, J. Membr. Sci. 495 (2015) 305–315, https://doi.org/10.1016/j.memsci.2015.08.025.
[15] S. Molina, J. Landaburu-Aguirre, L. Rodríguez-Sáez, R. García-Pacheco, J.G. de la Campa, E. García-Calvo, Effect of sodium hypochlorite exposure on polysulfone recycled UF membranes and their surface characterization, Polym. Degrad. Stab. 150 (2018) 46–56, https://doi.org/10.1016/j.polymdegradstab. 2018.02.012.
[16] A. Ramdani, A. Deratani, S. Taleb, N. Drouiche, H. Lounici, Performance of NF90 and NF270 Commercial Nanofiltration Membranes in the Defluoridation of Algerian Brackish Water, Desalin. Water Treat. 212 (2021) 286–296, https://doi.org/10.5004/dwt.2021.26680.
[17] R. Zhang, S. Su, S. Gao, J. Tian, Reconstruction of the polyamide film in nanofiltration membranes via the post-treatment with a ternary mixture of ethanol-water-NaOH: mechanism and effect, Desalination 519 (2021) 115317, https://doi.org/10.1016/j.desal.2021.115317.
[18] M. Mänttäri, T. Pekuri, M. Nyström, NF270, a new membrane having promising characteristics and being suitable for treatment of dilute effluents from the paper industry, J. Membr. Sci. 242 (1) (2004) 107–116, https://doi.org/10.1016/j.memsci.2003.08.032.
[19] I.S. Argyle, C.J. Wright, M.R. Bird, The effect of ethanol pre-treatment upon the mechanical, structural and surface modification of ultrafiltration membranes, Sep. Sci. Technol. 52 (12) (2017) 2040–2048, https://doi.org/10.1080/01496395.2017.1310234.
[20] M.M. Rahman, S. Al-Sulaimi, A.M. Farooque, Characterization of new and fouled SWRO membranes by ATR/FTIR spectroscopy, Appl Water Sci 8 (6) (2018) 183, https://doi.org/10.1007/s13201-018-0806-7.
[21] C.Y. Tang, Y.-N. Kwon, J.O. Leckie, Effect of membrane chemistry and coating layer on physiochemical properties of thin film composite polyamide RO and NF membranes: I. FTIR and XPS characterization of polyamide and coating layer chemistry, Desalination 242 (1) (2009) 149–167, https://doi.org/10.1016/j.desal.2008.04.003.
[22] C.Y. Tang, Y.-N. Kwon, J.O. Leckie, Effect of membrane chemistry and coating layer on physiochemical properties of thin film composite polyamide RO and NF membranes: II. Membrane physiochemical properties and their dependence on polyamide and coating layers, Desalination 242 (1) (2009) 168–182, https://doi.org/10.1016/j.desal.2008.04.004.
[23] W. Lee, C.H. Ahn, S. Hong, S. Kim, S. Lee, Y. Baek, et al., Evaluation of surface properties of reverse osmosis membranes on the initial biofouling stages under no filtration condition, J. Membr. Sci. 351 (1–2) (2010) 112–122, https://doi.org/10.1016/j.memsci.2010.01.035.
[24] S. Mondal, S.R. Wickramasinghe, Produced water treatment by nanofiltration and reverse osmosis membranes, J. Membr. Sci. 322 (1) (2008) 162–170, https://doi.org/10.1016/j.memsci.2008.05.039.
[25] V.T. Do, C.Y. Tang, M. Reinhard, J.O. Leckie, Degradation of polyamide Nanofiltration and reverse osmosis membranes by hypochlorite, Environ. Sci. Technol. 46 (2) (2012) 852–859, https://doi.org/10.1021/es203090y.
[26] I. Kammakakam, Z. Lai, Next-generation ultrafiltration membranes: a review of material design, properties, recent progress, and challenges, Chemosphere 316 (2023) 137669, https://doi.org/10.1016/j.chemosphere.2022.137669.
[27] E. Bormashenko, R. Pogreb, G. Whyman, Y. Bormashenko, R. Jager, T. Stein, et al., The reversible Giant change in the contact angle on the Polysulfone and

Polyethersulfone films exposed to UV irradiation, Langmuir 24 (12) (2008) 5977–5980, https://doi.org/10.1021/la800527q.
[28] R. García-Pacheco, J. Landaburu-Aguirre, A. Lejarazu-Larrañaga, L. Rodríguez-Sáez, S. Molina, T. Ransome, E. García-Calvo, Free chlorine exposure dose (ppm·h) and its impact on RO membranes ageing and recycling potential, Desalination 457 (2019) 133–143, https://doi.org/10.1016/j.desal.2019.01.030.
[29] B.Z. Sabio, R.G. Pacheco, P.V. Pàrraga, I.A. Bernades, H.M. Sales, G. Blandin, Gravity-driven ultrafiltration and Nanofiltration recycled membranes for tertiary treatment of urban wastewater, Journal of Water Process Engineering 63 (2024) 105545, https://doi.org/10.1016/j.jwpe.2024.105545.
[30] W. Lawler, A. Antony, M. Cran, M. Duke, G. Leslie, P. Le-Clech, Production and characterisation of UF membranes by chemical conversion of used RO membranes, J. Membr. Sci. 447 (2013) 203–211, https://doi.org/10.1016/j.memsci.2013.07.015.